Plasmonics (2015) 10:139–144
DOI 10.1007/s11468-014-9787-z

Tunable Multichannel Plasmonic Filter Based on Coupling-Induced Mode Splitting

Zhao Zhang · Fenghua Shi · Yihang Chen

Received: 17 June 2014 / Accepted: 25 August 2014 / Published online: 6 September 2014

Abstract Combining with tight-binding approach, novel multichannel plasmonic filters are designed by inserting identical coupled cavities between metal-insulator-metal waveguides. We show that the eigenmodes of the plasmonic cavities will asymmetrically split under their coupling with each other. Such an asymmetrical mode splitting provides strongly correlated transmission channels which can be manipulated simultaneously. All channels will red shift or blue shift with the changing of the lengths or widths of the rectangular cavities. The intervals of the channels can be tuned by adjusting the coupling strength of the cavities. Both finite difference time domain method and transfer matrix method are used to investigate the considered plasmonic system. Our results may have important applications in the fields of high-density plasmonic integration circuits and nonlinear plasmonic devices.

Keywords Surface plasmons · Filter · Integrated optics devices

Introduction

Surface plasmon polaritons (SPPs) are a type of surface waves, which travel along the metal-dielectric interface owing to the interaction between the free electrons in metal and the electromagnetic (EM) field in dielectric [1, 2]. SPPs are shorter in wavelength than the incident wave. Hence, SPPs can have tighter spatial confinement and higher local field intensity. They have the most promising applications in the highly integrated optical circuits and devices because of their ability to overcome the diffraction limit and manipulate the light on subwavelength scales [1–3]. Recently, nanoscale SPP-based photonic devices such as the all-optical switching [4], splitters [5], Y-shaped combiners [6], multimode interferometers [7], couplers [8], Mach-Zehnder interferometers [9], and Bragg reflectors [10–12] have been investigated both numerically and experimentally. Among these configurations, metal-insulator-metal (MIM) plasmonic waveguides attract more attention in the design of truly nanoscale photonic devices since they can realize deep-subwavelength confinement of light in relatively simple structure [13, 14]. Some plasmonic wavelength filtering structures based on MIM waveguides have been proposed and investigated, such as tooth-shaped waveguide filters [15], channel drop filters with disk [16], rectangular [17], and ring [18] resonators, as well as wavelength demultiplexers [19, 20]. However, these plasmonic structures only possess one filtering channel. Some other plasmonic filters with multiple channels were reported, such as multichannel bandstop filters with MIM Bragg gratings [21] and multichannel bandpass filters containing Bragg scattering units [22] or side-couple resonators with response of electromagnetically induced transparency [23]. However, practical applications of such plasmonic filters with Bragg gratings or resonant units are restricted owing to their geometrical complexity. More importantly, so far there is no effective method to design multichannel plasmonic filters, the transmission channels of which can be efficiently controlled.

In solid-state physics, tight-binding (TB) model is a method that can be used to calculate the electronic band structure and analyze the splitting of atomic energy level. The TB scheme was successfully used to explain the properties of photonic band gap structures [24–26]. It is anticipated that the TB model can also be applied to the plasmonic system. By introducing resonant cavities into the plasmonic system, it is

Zhao Zhang and Fenghua Shi contributed equally to this work.

Z. Zhang · F. Shi · Y. Chen (✉)
Laboratory of Quantum Information Technology, School of Physics and Telecommunication Engineering, South China Normal University, Guangzhou 510006, China
e-mail: yhchen@scnu.edu.cn

possible to create highly localized eigenmodes of the cavities, which are analogous to the states of the tightly bound electrons in solids. The coupling of these plasmonic eigenmodes, which can be analyzed from the TB model, may lead to novel properties required for the design of ultracompact plasmonic devices.

In this paper, we investigate the coupling effect between the identical cavities embedded in the MIM plasmonic system using both finite difference time domain (FDTD) method and transfer matrix method (TMM). Asymmetrical coupled-induced eigenmode splitting is observed, which can be well explained by the TB model. Based on such a mode splitting, we propose a novel multichannel plasmonic filter, the channels of which are correlated and can be efficiently manipulated.

Model and Simulation Methods

Consider a plasmonic structure constructed by embedding rectangular cavities between two SPP waveguides, as shown in Fig. 1. Suppose that transversal-magnetic (TM) SPP mode is excited and propagate along the metal-dielectric interfaces in the x direction. The dispersion relation of the fundamental TM mode in MIM structure can be written as [12, 21]

$$\varepsilon_{\mathrm{m}} k_{\mathrm{d}} \tanh\left(\frac{w k_d}{2}\right) + \varepsilon_{\mathrm{d}} k_{\mathrm{m}} = 0, \tag{1}$$

where w is the width of dielectric layer. ε_{d} and ε_{m} represent the permittivity of dielectric and metal. k_{d} and k_{m} are transverse propagation constants in the dielectric and the metal, respectively. They satisfy

$$k_{\mathrm{d}} = \sqrt{\beta^2 - \varepsilon_{\mathrm{d}} k_0^2}, \quad k_{\mathrm{m}} = \sqrt{\beta^2 - \varepsilon_{\mathrm{m}} k_0^2}, \tag{2}$$

where β is the propagation constant of the SPP; $k_0 = 2\pi/\lambda_0$ represents the wave number of light in free space. The effective index of the MIM plasmonic structure can be obtained from

$$n_{\mathrm{eff}} = \beta / k_0. \tag{3}$$

In our configurations, the metal is chosen as silver. The dielectric dispersion of the silver can be described by Drude model $\varepsilon_{\mathrm{m}}(\omega) = \varepsilon_\infty - \omega_p^2/[\omega(\omega + i\gamma)]$. Here, ε_∞ is the dielectric constant at the infinite frequency, ω_{P} is the bulk plasma frequency, and γ is the electron collision frequency. In the following simulations, the parameters for silver are set as $\varepsilon_\infty = 3.7$, $\omega_{\mathrm{P}} = 9.1$ eV, and $\gamma = 0.018$ eV [27].

It is well known that EM wave will decay exponentially as it propagates inside the metal because its wave number is imaginary. In our considered system, the metal baffles are set to be quite thin so that parts of the waves can tunnel through the baffles. Inside the cavities, the phase change per round-trip of the waves can be written as $\Delta\varphi = 4\pi n_{\mathrm{eff}} L/\lambda + \varphi_r$, where L is the length of the cavity. $\varphi_{\mathrm{r}} = \varphi_{\mathrm{L}} + \varphi_{\mathrm{R}}$, where φ_L and φ_R are respectively the reflection phase changes of the waves at the left and right ends of the cavity. Stable standing wave will build up constructively in the cavity when $\Delta\varphi = 2j\pi$ is satisfied. Here, j is an integer. Therefore, we can obtain the wavelengths of the eigenmodes of the plasmonic cavity [28, 29].

$$\lambda_j = \frac{2 n_{\mathrm{eff}} L}{(j - \varphi_{\mathrm{r}}/\pi)}. \tag{4}$$

Both finite difference time domain (FDTD) method [30] and transfer matrix method (TMM) [31, 32] will be used to investigate the properties of the considered system. In TMM simulations, the amplitudes of the electric components of the

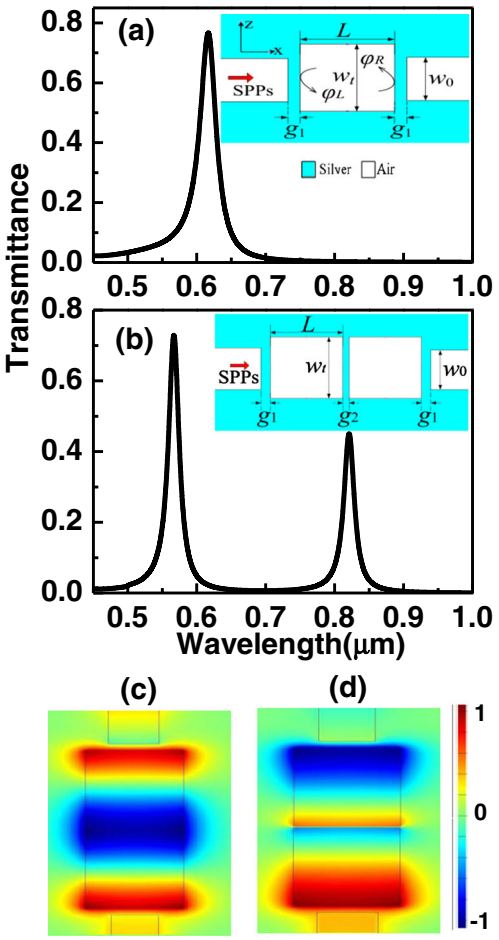

Fig. 1 Transmission spectra obtained from FDTD method for the MIM plasmonic system embedded with **a** one cavity and **b** two cavities, respectively. The *insets* show the configurations of the plasmonic systems. The dimensions are $g_1 = 20$ nm, $g_2 = 5$ nm, $L = 200$ nm, $w_0 = 50$ nm, and $w_{\mathrm{t}} = 100$ nm. Magnetic field distributions corresponding to the **c** symmetric mode at 567 nm and **d** antisymmetric mode at 820 nm for the system of (**b**)

forward and backward waves can be related via a transfer matrix

$$\begin{bmatrix} \cos(k_m g) & i/q_m \sin(k_m g) \\ iq_m \sin(k_m g) & \cos(k_m g) \end{bmatrix} \quad (5)$$

for the metal baffle, and another matrix

$$\begin{bmatrix} \cos(k_c L) & i/q_c \sin(k_c L) \\ iq_c \sin(k_c L) & \cos(k_c L) \end{bmatrix} \quad (6)$$

for the cavity. Here, $k_m = \omega\sqrt{\varepsilon_m}$, $k_c = \omega n_{eff}$, $q_m = \sqrt{\varepsilon_m}$, $q_c = n_{eff}$, g is the width of the metal baffle. Suppose that the matrix connecting the incident end and the exit end is X_N, the transmittance of the plasmonic system can be written as

$$T = \left| \frac{2}{x_{11} + x_{22} - x_{21} - x_{12}} \right|^2, \quad (7)$$

where x_{ab}(a,b=1,2) are the matrix elements of X_N.

Numerical Simulations and Discussions

We first investigate the plasmonic system embedded with a single cavity. In Fig. 1a, the width of the waveguide w_0 is set as 50 nm, the length L and width w_t of the rectangular cavity are 200 and 100 nm, and the width of the metal baffle g_1 is 20 nm. FDTD method with perfectly matched layer absorbing boundary condition is used to simulate the transmission response. The grid sizes in the x and z directions are set to be 1 and 5 nm. A fundamental TM mode of the plasmonic waveguide is excited and propagates along the waveguide. It is seen from Fig. 1a that a transmission channel corresponding to an eigenmode of the resonant cavity appears at 637 nm. Such an eigenmode can also be described by Eq. (4).

Next, we insert two identical cavities between the MIM waveguides, as shown in Fig. 1b. Here, we assume that the metal baffle between the two cavities has a width g_2 of 5 nm. Since the distance between the cavities is very short, strong coupling between the eigenmodes of the cavities will establish. According to the TB model [25, 26], such a strong coupling can lead to the splitting of the eigenmodes. Hence, two transmission modes appear in Fig. 1b. Our system is analogous to the diatomic molecules [33], where the interaction between the atoms results in the splitting of the degenerate atomic orbitals into symmetric and antisymmetric orbitals. In Fig. 1b, the mode with lower energy at longer wavelength 820 nm should be the antisymmetric coupling mode, while the mode with higher energy at shorter wavelength 567 nm should be the symmetric coupling mode. For verification, Fig. 1c, d presents the spatial distribution of magnetic field corresponding

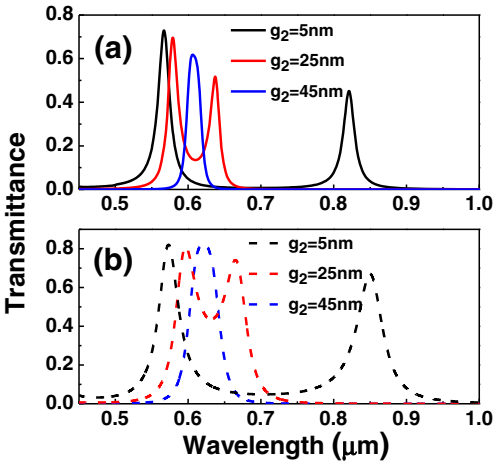

Fig. 2 Transmission spectra obtained from **a** FDTD method and **b** TMM under different g_2 for the dual cavity plasmonic system with g_1=20 nm, L=200 nm, w_0=50 nm, and w_t=100 nm

to the two resonance modes. The symmetric (out of phase) and antisymmetric (in phase) field distributions can be observed at 567 and 820 nm, respectively. It is also noted that the two modes in Fig. 1b do not locate symmetrically in the center of the original eigenmode in Fig. 1a. This can be understood from the resonant condition of Eq. (4). In Eq. (4), the wavelengths of the eigenmodes depend on the reflection phase change φ_r ($=\varphi_L+\varphi_R$). On the other hand, the values of φ_L and φ_R have a strong dependence on both g_1 and g_2 when the metal baffles are quite thin. Hence, φ_r of the cavities in Fig. 1b is not the same as that of the cavity in Fig. 1a, resulting in the difference between the center wavelength of the two modes in Fig. 1b and the wavelength of the eigenmode in Fig. 1a.

To further understand the mode splitting of the considered plasmonic system, the relationship between the structural parameters of our system and the transmission modes is investigated. Figure 2 shows the transmission spectra simulated from both FDTD method and TMM for the system with

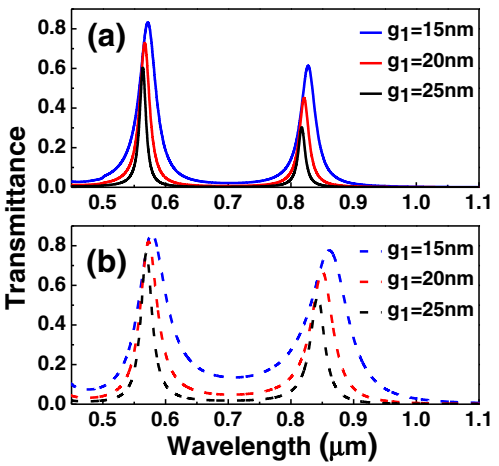

Fig. 3 Transmission spectra obtained from **a** FDTD method and **b** TMM under different g_1 for the dual cavity plasmonic system with g_2=5 nm, L=200 nm, w_0=50 nm, and w_t=100 nm

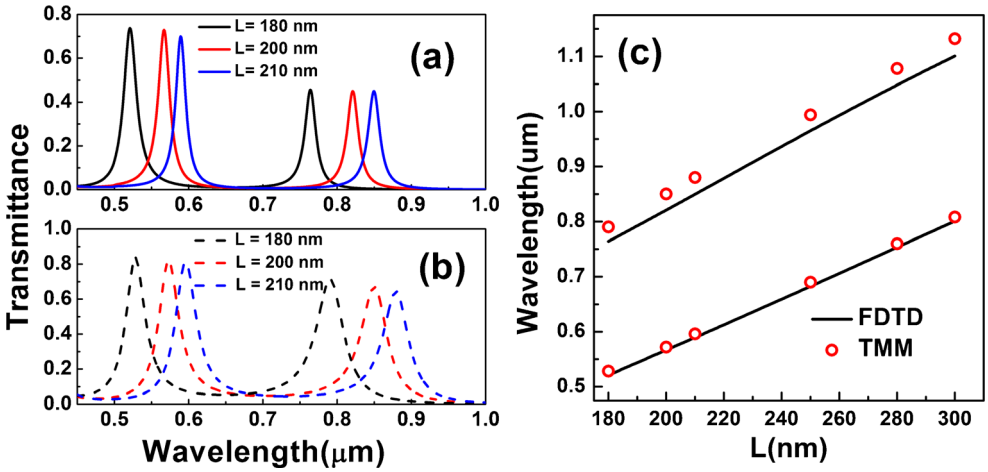

Fig. 4 Transmission spectra obtained from **a** FDTD method and **b** TMM for the dual cavity plasmonic system with different L. **c** Dependence of the two transmission modes on the lengths of the cavities L. The other geometrical parameters are g_1=20 nm, g_2=5 nm, w_0=50 nm, and w_t=100 nm

two identical cavities under different values of g_2. Here, the other structural parameters are the same as those in Fig. 1b. As shown in Fig. 2, the two transmission modes approach to each other as g_2 increases. When g_2 increases to 45 nm, they merge into one another. This phenomenon can also be understood from the TB model. The larger the distance (g_2) between the cavities is, the weaker the coupling of the eigenmodes of the cavities will be. When the value of g_2 becomes quite large, the coupling will be very weak and the eigenmodes will be degenerate. In Fig. 2, the simulated results from the FDTD method agree well with those from the TMM except for the transmittance of the transmission peaks. Furthermore, we can see from Fig. 2 that the center wavelength of the two split eigenmodes in structure with g_2=5 nm is obviously different to the wavelength of the degenerate modes in structure with g_2=45 nm. This can also be attributed to the dependence of the reflection phase shift φ_r of the cavities on the width of the metal baffle g_2, which has been discussed above.

The mode splitting induced by the coupling of the eigenmodes allows simultaneously control of the plasmonic transmission channels by adjusting the coupling strength between the resonant cavities. Moreover, it can be noticed from Fig. 2 that one split mode is much closer to the original eigenmode than the other one. The mode with larger wavelength is quite sensitive to the coupling strength; it shifts quickly to higher wavelength region as g_2 decreases. Such asymmetrical mode splitting is very useful in designing nonlinear plasmonic devices, such as plasmonic switches, logic gates, and plasmonic bistable memory devices [34], in which nonlinear effect is adjusted by manipulating the coupling strength.

It can be seen from Fig. 2 that there are some differences of the simulation results between the TMM and FDTD method. These differences are the result of the different parameters of silver used in these two methods. Compared to the FDTD method, where the measured parameters for silver are used in the simulations, TMM uses the ideal Drude model with less dissipation to describe the dielectric dispersion of the silver. Hence, broader resonances with higher transmittance are observed in the TMM-simulated results.

Influence of the value of g_1 on the filtering properties of the plasmonic system is also studied, as shown in Fig. 3. It is seen that the changes of g_1 will greatly affect the transmittances and the quality factors of the transmission modes rather than their locations. As g_1 increases, the transmittance decreases while the quality factor increases for the two modes. The reason for this phenomenon is that the baffle width g_1, related with the

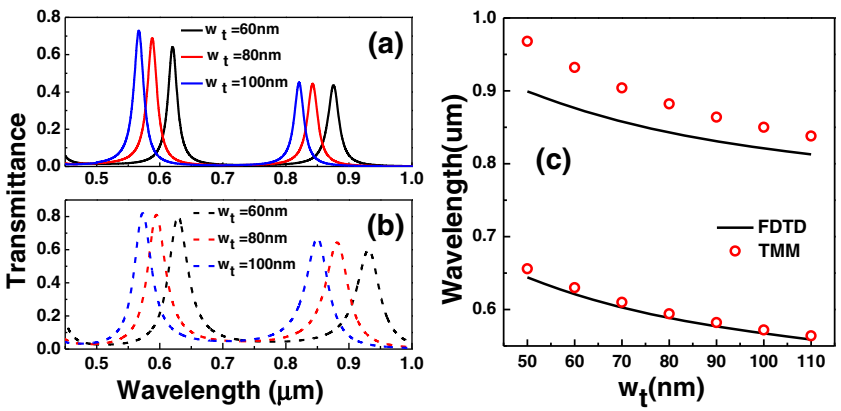

Fig. 5 Transmission spectra obtained from **a** FDTD method and **b** TMM for the dual cavity plasmonic system with different w_t. **c** Dependence of the two transmission modes on the widths of the cavities w_t. The other geometrical parameters are g_1= 20 nm, g_2=5 nm, L=200 nm, and w_0=50 nm

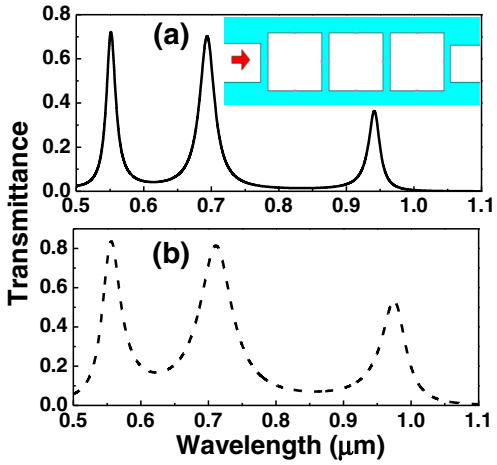

Fig. 6 Transmission spectra simulated from **a** FDTD method. **b** TMM for the plasmonic system embedded with three resonant cavities. The structural parameters are g_1=15 nm, g_2=5 nm, L=200 nm, w_0=50 nm, and w_t=100 nm

coupling strength between the waveguide and the cavity, does not influence the wavelengths of the two eigenmodes. With the increasing of g_1, more energy is dissipated inside the metal baffles, the transmittances hence decrease.

We then change the shape of the cavities and investigate the transmission properties of the filtering structure. Figure 4 shows the dependence of the two transmission modes on the cavity length L. It is seen that both the symmetric coupling mode (at shorter wavelength) and the antisymmetric coupling mode (at longer wavelength) shift to the longer wavelength region as L increases. This relationship between L and the resonant wavelengths is in accordance with that in Eq. (4). The wavelengths of the transmission modes as functions of the cavity width w_t are shown in Fig. 5. We can see that both the wavelengths of symmetric and antisymmetric coupling modes decrease as w_t increases. Such a phenomenon is the result of the changes of n_{eff} of the plasmonic cavities. From Eqs. (1) to (3) or Ref. [33], we can obtain that the value of n_{eff} of a MIM channel structure is inversely proportional to the width of the dielectric channel. Therefore, as w_t increases, n_{eff} of the plasmonic cavities decreases, and the resonant wavelengths obtained from Eq. (4) decreases as well.

Next, we insert three cavities between the two MIM waveguides and investigate the changes of the mode splitting, as shown in Fig. 6. Here, the widths of the two metal baffles between the waveguides and the cavities are both set to be g_1= 15 nm, and the widths of the metal baffles between the cavities are all set to be g_2=5 nm. It is seen from Fig. 6 that three transmission modes appear. This can be well explained by the TB model. Every plasmonic cavity has a corresponding resonance mode (as shown in Fig. 1a), that is, an eigenmode. When multiple cavities are brought together and arranged at a certain interval, previous degenerate eigenmodes will split due to the coupling with each other. According to the TB description, the number of the split modes should be equal to the number of the localized cavities. The theoretical treatment for the coupling of the eigenmodes can be found in Ref. [24]. Similarly, more transmission modes can be generated by introducing more coupled cavities into the plasmonic structure. The location and interval of these plasmonic channels can be manipulated, in the similar way as the two-cavity system, by adjusting the structural parameters. Therefore, the coupled cavities-based structures are useful for the design of multichannel plasmonic filters.

Conclusions

In conclusion, we have designed a novel type of multichannel plasmonic filters by introducing coupled resonant cavities between the MIM plasmonic waveguides. From the numerical results of FDTD method and TMM, asymmetrical eigenmode splitting is observed in the considered system. The split transmission modes are strongly correlated because of the coupling between the cavities. The wavelengths, wavelength interval, and number of the plasmonic transmission modes can be tuned as desired by adjusting the structural parameters of the proposed system. Tight-binding model is successfully used to understand the eigenmode splitting and can provide guidance for designing plasmonic filter with specific transmission channels. The proposed configuration of the multichannel filter has an ultracompact size with a length of a few hundred nanometers. Therefore, our results may find significant applications in highly integrated dense wavelength division multiplexing systems. Furthermore, the asymmetrical mode splitting is also useful for designing nonlinear plasmonic devices.

Acknowledgments This work was supported by National Natural Science Foundation of China (Grant No. 11274126) and Natural Science Foundation of Guangdong Province of China (Grant No. 9151063101000040).

References

1. Barnes WL, Dereux A, Ebbesen TW (2003) Surface plasmon subwavelength optics. Nature 424:824–830
2. Raether H (1988) Surface plasmons on smooth and rough surfaces and on gratings. Springer, Berlin
3. Genet C, Ebbesen TW (2007) Light in tiny holes. Nature 445:39–46
4. Lu H, Liu XM, Wang LR, Gong YR, Mao D (2011) Ultrafast all-optical switching in nanoplasmonic waveguide with Kerr nonlinear resonator. Opt Express 19:2910–2915
5. Veronis G, Fan S (2005) Bends and splitters in metal-dielectric-metal subwavelength plasmonic waveguides. Appl Phys Lett 87:131102
6. Gao HT, Shi HF, Wang CT, Du CL, Luo XG, Deng QL, Lin XD, Yao HM (2005) Surface plasmon polaritons propagation and combination in Y-shaped metallic channels. Opt Express 13: 10795–10800

7. Han ZH, He SL (2007) Multimode interference effect in plasmonic subwavelength waveguides and an ultra-compact power splitter. Opt Commun 278:199–203
8. Zhao HW, Guang HJT (2008) Novel optical directional coupler based on surface plasmon polaritons. Phys E 40:3025–3029
9. Han ZH, Liu L, Forsberg E (2006) Ultra-compact directional couplers and Mach-Zehnder interferometers employing surface plasmon polaritons. Opt Commun 259:690–695
10. Ditlbacher H, Krenn JR, Schider G, Leitner A, Aussenegg FR (2002) Two-dimensional optics with surface plasmon polaritons. Appl Phys Lett 81:1762–1764
11. Park J, Kim H, Lee B (2008) High order plasmonic Bragg reflection in the metal-insulator-metal waveguide Bragg grating. Opt Express 16:413–425
12. Han ZH, Forsberg E, He SL (2007) Surface plasmon Bragg gratings formed in metal–insulator–metal waveguides. IEEE Photon Technol Lett 19:91–93
13. Neutens P, Dorpe PV, Vlaminck I, Lagae L, Borghs G (2009) Electrical detection of confined gap plasmons in metal-insulator-metal waveguides. Nat Photonics 3:283–286
14. Zia R, Schuller J, Chandran BM (2006) Plasmonics: the next chip-scale technology. Mater Today 9:20–27
15. Lin XS, Huang XG (2008) Tooth-shaped plasmonic waveguide filters with nanometeric sizes. Opt Lett 33:2874–2876
16. Xiao SS, Liu L, Qiu M (2006) Resonator channel drop filters in a plasmon-polaritons metal. Opt Express 14:2932–2937
17. Hosseini A, Massoud Y (2007) Nanoscale surface Plasmon based resonator using rectangular geometry. Appl Phys Lett 90:181102
18. Wang TB, Wen XW, Yin CP, Wang HZ (2009) The transmission characteristics of surface plasmon polaritons in ring resonator. Opt Express 17:24096–24101
19. Noual A, Akjouj A, Pennec Y, Gillet JN, Djafari-Rouhani B (2009) Modeling of two-dimensional nanoscale Y-bent plasmonic waveguides with cavities for demultiplexing of the telecommunication wavelengths. New J Phys 11:103020
20. Lu H, Liu XM, Gong YK, Mao D, Wang LR (2011) Enhancement of transmission efficiency of nanoplasmonic wavelength demultiplexer based on channel drop filters and reflection nanocavities. Opt Express 19:12885–12890
21. Gong YK, Liu XM, Wang LR (2010) High-channel-count plasmonic filter with the metal-insulator-metal Fibonacci-sequence gratings. Opt Lett 35:285–287
22. Luo X, Zou XH, Li XF, Zhou Z, Pan W, Yan LS, Wen KH (2013) High-uniformity multichannel plasmonic filter using linearly lengthened insulators in metal-insulator-metal waveguide. Opt Lett 38: 1585–1587
23. Lu H, Liu XM, Wang GX, Mao D (2012) Tunable high-channel-count bandpass plasmonic filters based on an analogue of electromagnetically induced transparency. Nanotechnology 23:444003
24. Lidorikis E, Sigalas MM, Economou EN, Soukoulis CM (1998) Tight-binding parametrization for photonic band gap materials. Phys Rev Lett 81:1405–1408
25. Bayindir M, Temelkuran B, Ozbay E (2000) Tight-binding description of the coupled defect modes in three-dimensional photonic crystals. Phys Rev Lett 84:2140–2143
26. Chen YH, Dong JW, Wang HZ (2006) Omnidirectional resonance modes in photonic crystal heterostructures containing single-negative materials. J Opt Soc Am B 23:2237–2240
27. Palik GP (1985) Handbook of optical constants of solids. Academic, Boston
28. Zhang Q, Huang XG, Lin XS, Tao J, Jin XP (2009) A subwavelength coupler-type MIM optical filter. Opt Express 17:7549–7554
29. Tao J, Huang XG, Zhu JH (2010) A wavelength demultiplexing structure based on metal-dielectric-metal plasmonic nano-capillary resonators. Opt Express 18:11111–11116
30. Taflove A, Hagness SC (2000) Computational electrodynamics: the finite-difference time-domain method. Artech House Publishers, Boston
31. Bethune DS (1989) Optical harmonic generation and mixing in multilayer media: analysis using optical transfer matrix techniques. J Opt Soc Am B 6:910–916
32. Born M, Wolf E (1999) Principles of optics. University Cambridge, Cambridge
33. Ashcroft NW, Mermin ND (1976) Solid State Physics. Sounders, Philadelphia
34. Khitrova G, Gibbs HM (1999) Nonlinear optics of normal-mode-coupling semiconductor microcavities. Rev Mod Phys 71:1591–1639